Hindawi
Shock and Vibration
Volume 2020, Article ID 4182094, 16 pages
https://doi.org/10.1155/2020/4182094

Research Article

Enhancing the Seismic Performance of Precast RC Frames with Cladding Panels through Setting U-Shaped Dampers and Rocking Walls

Qing Jiang[1,2], **Hanqin Wang**[1], **Yulong Feng**[1,2], **Xun Chong**[1,2], **Junqi Huang**[1,2] and **Yibo Liu**[1]

[1]*School of Civil Engineering, Hefei University of Technology, Hefei 230009, Anhui, China*
[2]*Anhui Civil Engineering Structures and Materials Laboratory, Hefei 230009, Anhui, China*

Correspondence should be addressed to Yulong Feng; feng_yulong@126.com

Received 21 February 2020; Revised 17 May 2020; Accepted 22 May 2020; Published 16 June 2020

Academic Editor: Alfredo Reyes-Salazar

An approach combining U-shaped dampers (USDs) and rocking walls is proposed in this paper to improve the seismic performance of traditional precast reinforced concrete (RC) frames with cladding panels (PRCFCPs): (1) the steel bar and USD connection methods are adopted at the top and bottom of the cladding panels to use the relative deformation between the cladding panels and the main structure and then dissipate the seismic energy and (2) rocking walls are added to the structure to control the structural deformation profiles. The USD numerical model is calibrated using the test data, and a series of nonlinear pushover analyses, dynamic time-history analyses, and incremental dynamic analyses are successively performed to compare the seismic performance and collapse capacity of the PRCFCP, PRCFCP with USDs (PRCFCP-USD), and PRCFCP with USDs and rocking walls (PRCFCP-USD-RW).The results show that the USDs in the PRCFCP-USD-RW undergo more uniform deformation along the structural height and higher energy dissipation efficiency and the PRCFCP-USD-RW exhibits enhanced seismic performance and collapse capacity, which verify the superiority of the proposed combined approach.

1. Introduction

Precast concrete cladding panels (PCCPs), fabricated at manufacturing plants and assembled on a supporting main structure at the project site, have been widely used as an architectural external wall system during the past several decades [1]. Losch et al. [2] described the art of precast/prestressed concrete sandwich wall panels and noted that the use of this kind of PCCP has become more widespread in the United States. According to the current design specification [3, 4], PCCPs are primarily designed as a nonstructural member to bear their self-weight and out-of-plane loads, including seismic and wind loads.

Belleri et al. [5] summarized the vulnerabilities of the cladding panels following major earthquakes in the Italian territory and noted that the interaction between the cladding panels and the main structure was a noticeable vulnerability of the structure. The connection details between the cladding panels and the supporting structure significantly affect their interaction, which might reduce the performance and safety of both panels and main structure [6, 7]. To mitigate the interaction and reduce the sensitivity of the PCCP to the deformation of the main structure, the Precast Concrete Institute (PCI) recommends that the force transmission path from the cladding panel to the main structure should be statically determinate, each cladding panel should not be more than two gravity-bearing connections, and those connections should be placed in the same horizontal position [3]. Thus, the commonly used connection form is a four-point flexible connection, including two gravity-bearing connection points and two lateral force-bearing connection points. At present, the steel bar and limiting device connection methods are adopted at the top and bottom of the cladding panels in China [4], as shown in Figure 1(a),

where the steel bars are placed at the top of the cladding panel and protrude into the floor cast-in-place layer; limiting devices constructed by angle steel are connected with the cladding panel and main structure by long bolts. The steel bar and limiting device connection can resist out-of-plane displacement of the cladding panel and prompt the cladding panel sliding in-plane. The PCCPs with the aforementioned connection forms will exhibit sliding or rocking deformation under an earthquake. These deformation modes are recommended to coordinate the deformation of the main structure and reduce the interaction between the cladding panels and the main structure to enhance the structural safety [8].

Accordingly, there is a relative deformation between the cladding panels and the main structure, in which various energy dissipaters were arranged by many scholars to improve the seismic performance of the structures with PCCPs. Tyler [9] used polytetrafluoroethylene sliding joints to separate the cladding panels from the main structure of a building and noted that their use enables the damping of earthquake and wind motions. Cohen and Powell [10] classified the energy-consuming connections around the cladding panels and studied the design methods of these connections. Pinelli et al. [11] connected the cladding panel and the main structure by an elliptical soft steel energy dissipater. The test and finite element analyses showed that the performance of this energy-dissipating connection form was stable. Ferrara et al. [12] experimentally evaluated the behaviour of friction dampers to be used along the edges of the cladding panels in precast reinforced concrete (RC) buildings. Baird et al. [13] installed U-shaped flexural plates at the lateral connection point of the four-point connected cladding panel and found that the U-shaped flexural plates can effectively dissipate seismic energy and reduce the deformation of the structure under earthquakes. Negro and Lamperti Tornaghi [14] investigated PCCPs with friction-based devices, and the reliability was confirmed by several tests. Lago et al. [15, 16] proposed a steel w-shaped folded plate dissipative connector and a multiple-slit device for the PCCPs. The test results showed that the proposed devices can be effectively used for precast RC structures with cladding panels. Karadoğan et al. [17] arranged steel cushions that have excellent dissipation capacity between the main structure and PCCPs. The test results showed that the plastic deformations accumulated on the steel cushions, and no damage was observed on the PCCPs; using bolts to connect the steel cushions and PCCPs is a reliable connection technique.

The soft-storey failure of RC frames has been mentioned by some existing studies, and rocking systems have proven to be an effective means to control the structural deformation and damage distribution [18, 19]. In particular, the rocking systems and the energy dissipaters have been frequently combined to obtain enhanced seismic performance structures. Deierlein et al. [20] proposed an earthquake resilient rocking steel frame system with energy-dissipating fuses and confirmed that the system can sustain extreme earthquake ground shaking without structural damage. Wada et al. [21] retrofitted the G3 teaching building at Tokyo Industrial University with rocking walls and steel dampers. This structure survived the 2011 Miyagi earthquake. Twigdenand and Henry [22] experimentally investigated a posttensioned rocking wall with energy-dissipating O-connectors attached along the vertical. Zhang et al. [23] combined precast rocking walls and friction dampers or buckling-restrained braces to form an inertial force-limiting floor anchorage system that is a low-damage seismic-resistant system. Feng et al. [24] used rocking walls to mitigate the drift concentration issue of buckling-restrained braced frames. Rahgozar et al. [25] numerically investigated the effects of soil-foundation modelling on the seismic performance of rocking braced frames with butterfly-shaped fuses. These studies indicated that the rocking systems might make the energy dissipaters work more effectively.

In this paper, in order to retrofit the existing structure of the precast RC frame with cladding panels (PRCFCPs), U-shaped dampers (USDs) that were developed in 1972 by Kelly et al. [26] and rocking walls are added into a PRCFCP to form a damping and damage-controlling system. This paper focuses on the effect of the USDs and rocking walls on the seismic performance of the PRCFCP through numerical investigations and comparative analyses. A series of nonlinear pushover analyses, dynamic time-history analyses, and incremental dynamic analyses are performed to compare the seismic performance and the seismic collapse capacity of the PRCFCP, PRCFCP with the USDs (PRCFCP-USD), and PRCFCP with the USDs and rocking walls (PRCFCP-USD-RW).

2. Description of the Structural System

2.1. Connection Details. Figure 1(b) shows a connection detail of the proposed damping cladding panels. A precast concrete sandwich wall panel is used as the cladding panel and connected to the main structure at each storey. The cladding panel is connected to the upper and down floors through a row of steel bars and USDs at the top and bottom of the cladding panel, which are deemed the steel bar and USD connection methods, respectively. The USDs are connected to other members through high-strength bolts [17, 27]. In this steel bar connection method, two layers of steel bars are placed at the top of the cladding panel and protrude into the floor cast-in-place layer, and then a fixed constraint end is formed to resist out-of-plane loads. Thus, the construction quality and earthquake safety are easily guaranteed. For the entire cladding panel that spans a single storey using these connection methods, the deformation mode under a horizontal earthquake is dominated by horizontal sliding deformation at the bottom of the cladding panel. Thus, the USDs that are set in the places where USDs undergo horizontal sliding deformations can dissipate energy through their own plastic deformations, as shown in Figure 1(c).

2.2. Structural Systems. Figure 2 describes the schematic of PRCFCP-USD-RW as a retrofitting structure of PRCFCP, which consists of a precast RC frame with the proposed

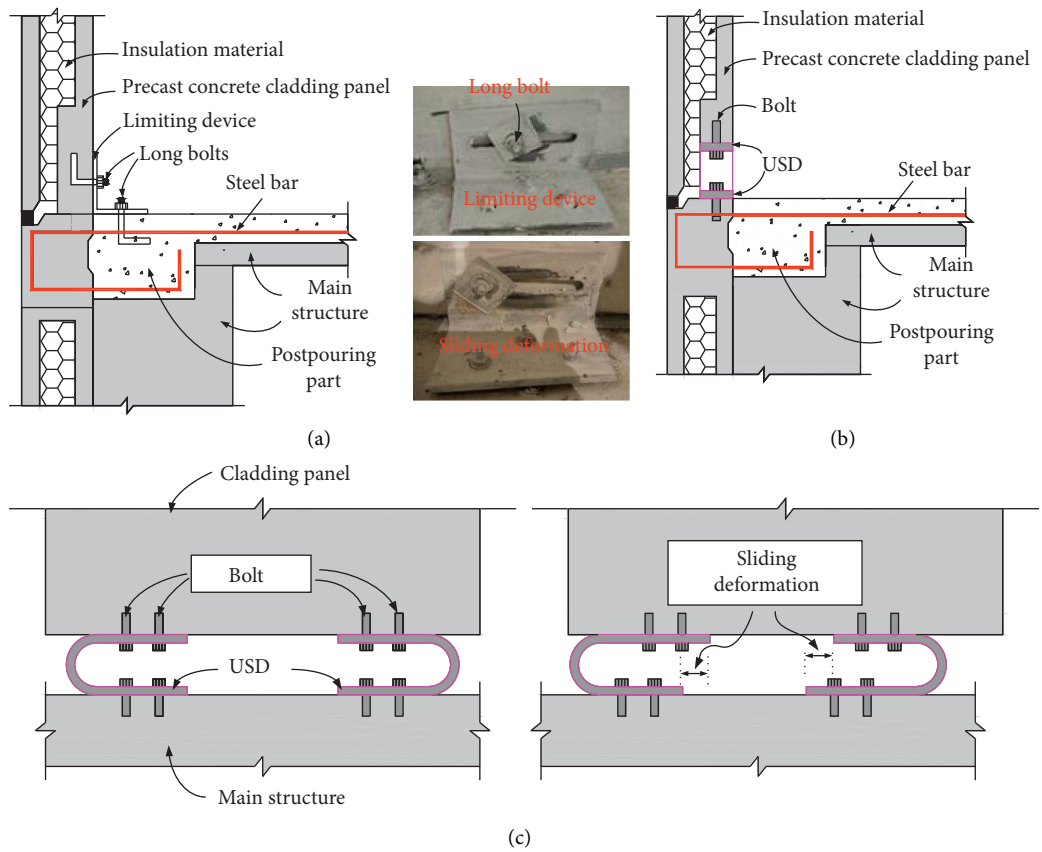

Figure 1: Connection details and deformation mode of the proposed damping cladding panel. (a) Typical cladding connection 2 in China. (b) Connection details. (c) Deformation mode of the proposed damping cladding panel.

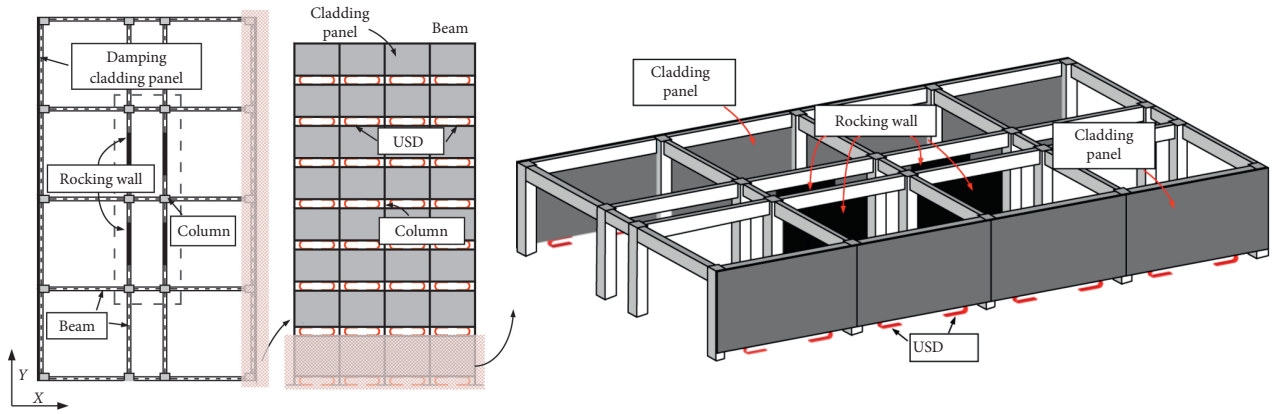

Figure 2: Schematic of a PRCFCP-USD-RW system.

cladding panels, as shown in Figure 1, and some rocking walls are attached only to beams at the middle of the structure in the Y direction. The cladding panels in the PRCFCP-USD-RW are no longer a nonstructural element but are a support member of the USDs. Together with the USDs, a shock absorbing unit is formed to transmit the interstorey drift generated by the earthquake to the USDs, and the plastic deformation of the USDs is used to dissipate the seismic energy to reduce the main structural damage. The rocking walls can render the storey drift of the structure uniform. When the storey drift is uniform, the USDs at each storey can exert an energy dissipation capacity. The collaboration between the USDs and the rocking walls plays a dual role in coordinating the interstorey drift and energy dissipation to achieve a controllable damage degree and distribution.

3. Contrast Models and Finite Element Models

3.1. Calibration of the USD Model. OpenSees [28] numerical simulation software is used for the nonlinear analysis in this paper. The definition of the USD parameters in the model is based on the force-displacement curve obtained from a test performed by the authors. Figure 3(a) shows the USD test model and loading device. The length, width, height, and thickness of the USD are 276 mm, 70 mm, 174 mm, and 12 mm, respectively. The material of the USD is Q235 steel (GB50017-2003) [29]. Figure 3(b) shows the loading protocol in this test. The loading amplitude displacements of each stage are 3 mm, 7 mm, 14 mm, 28 mm, 42 mm, and 60 mm, respectively. The front five stages are cycled three times, and the last stage is cycled approximately 18 times. The USD in OpenSees uses the Steel02 model and the zero-length element for the simulation [30]. The Steel02 model has a yield force $F_y = 11.97$ kN and initial elastic stiffness $E = 3.99$ kN/mm. The parameters controlling the transition from the elastic stage to the plastic stage are as follows: $R_0 = 20$, $CR_1 = 0.925$, and $CR_2 = 0.15$. Additionally, the isotropic hardening parameters are $a_1 = 0.25$, $a_2 = 5$, $a_3 = 0.25$, and $a_4 = 5$. The definition of these parameters can be found in [28]. Figure 3(c) shows the comparison of force-displacement curves between the simulations and the experiments. The simulated results are basically consistent with the experimental results, indicating that the USD model parameters are set properly.

3.2. Contrast Models. Figure 4(a) shows an 8-storey RC frame structure from [31]. The 8-storey RC frame was designed based on existing Chinese code for the design of concrete structures and seismic design of buildings. However, the soft-storey also occurred in this baseline building under horizontal earthquake loads and can be prevented by the addition of rocking walls, which is the reason to use this 8-storey RC frame herein as a benchmark model to construct other contrast models. The structural plane is a rectangle of 24 m by 50.4 m, and the column spacing is 7.5 m or 3.0 m. The earthquake resisting system of the benchmark model comprises five and four moment-resisting frames (MRFs) at the transverse and longitudinal directions of the structure (X and Y directions), respectively. The first and second storeys have heights of 4.5 m and 4.0 m, respectively, and the upper storeys have a height of 3.5 m, resulting in a total height of 29.5 m. The benchmark model is designed for a seismic area with Site Classification II and design ground Group 1, classified as a zone of intensity 8, with a basic design peak ground acceleration (PGA) of 0.2 g. Two concrete strength grades were adopted, C40 for all beams and floors and C45 for all columns (i.e., the cubic compressive strengths of the concrete are 40 MPa and 45 MPa, resp.). HRB 400 reinforcement (i.e., hot rolled ribbed reinforcement with a yield strength of 400 MPa) was adopted for the longitudinal mild steel reinforcement of beams, floors, and columns. The thickness of all floors was 100 mm, and the distribution steel reinforcements bilaterally distributed were allφ10@200 (φ10 means that the diameter of distribution steel reinforcements is 8 mm; @200 means that the spaces of distribution steel reinforcement are 200 mm). All columns and beams used rigid connections. More information regarding this frame structure, such as the beam-column section size and reinforcement, and design dead and live loads, can be found in [31].

To illustrate the performance advantages of the proposed PRCFCP-USD-RW, three different contrast models are developed based on the benchmark model. Only the Y direction seismic action is considered; thus, the comparison model considers only the addition of the rocking walls and the cladding panels in the Y direction, and the earthquake resisting system in the X direction is the same as the benchmark model. The traditional and damping cladding panels are added to the benchmark model in the Y direction, and the PRCFCP and PRCFCP-USD models are created, as shown in Figures 4(b) and 4(c), respectively. The traditional cladding panels at the bottom are connected by two limiting devices that allow the panel to slide freely under design displacement. In the PRCFCP-USD model, four USDs are arranged at the bottom of each cladding panel, and the size and material of each USD are the same as those shown in Figure 3(a). Furthermore, four rocking walls are added to the PRCFCP-USD model in the Y direction, and the PRCFCP-USD-RW model is formed, as shown in Figure 4(d). The sectional dimension of the rocking walls is the same as that in [31], which is 3600 mm × 150 mm. The paper focuses on the seismic responses of three comparison models, i.e., PRCFCP, PRCFCP-USD, and PRCFCP-USD-RW.

3.3. Finite Element Models. Figure 5 schematically shows the finite element model of the PRCFCP-USD-RW. The benchmark, PRCFCP, and PRCFCP-USD finite element models are modelled using the same techniques. In this paper, the RC beams, columns, and rocking walls are modelled via displacement-based beam-column (dispBeamColumn) fibre elements, in which their concrete and steel reinforcement materials use Concrete01 (because the tensile strength is less than the compressive strength, Concrete01 is used to build model) and Steel02 (the elastic tangent of reinforcement is 200 GPa, and strain-hardening ratio is 0.01), respectively. Some approaches have been proposed to model the panels (or walls) such as the multilayer element [32] or rigid beam element [33] with the bottom linked by a nonlinear zero-length element. The cladding panels and floors are simulated by shell elements, and the material adopts an elastic model. Notably, the shell elements for cladding panels are not connected to the adjacent columns, and the master nodes of rigid diaphragm at each storey were set in the structural centroid. The limiting devices in the PRCFCP and the USDs in the PRCFCP-USD and PRCFCP-USD-RW are simulated by zero-length elements, which replaces the translational constraint in the loading direction by a Steel02 material defining the force-displacement relationship shown in Section 3.1. The finite element models for the PRCFCP-USD and PRCFCP-USD-

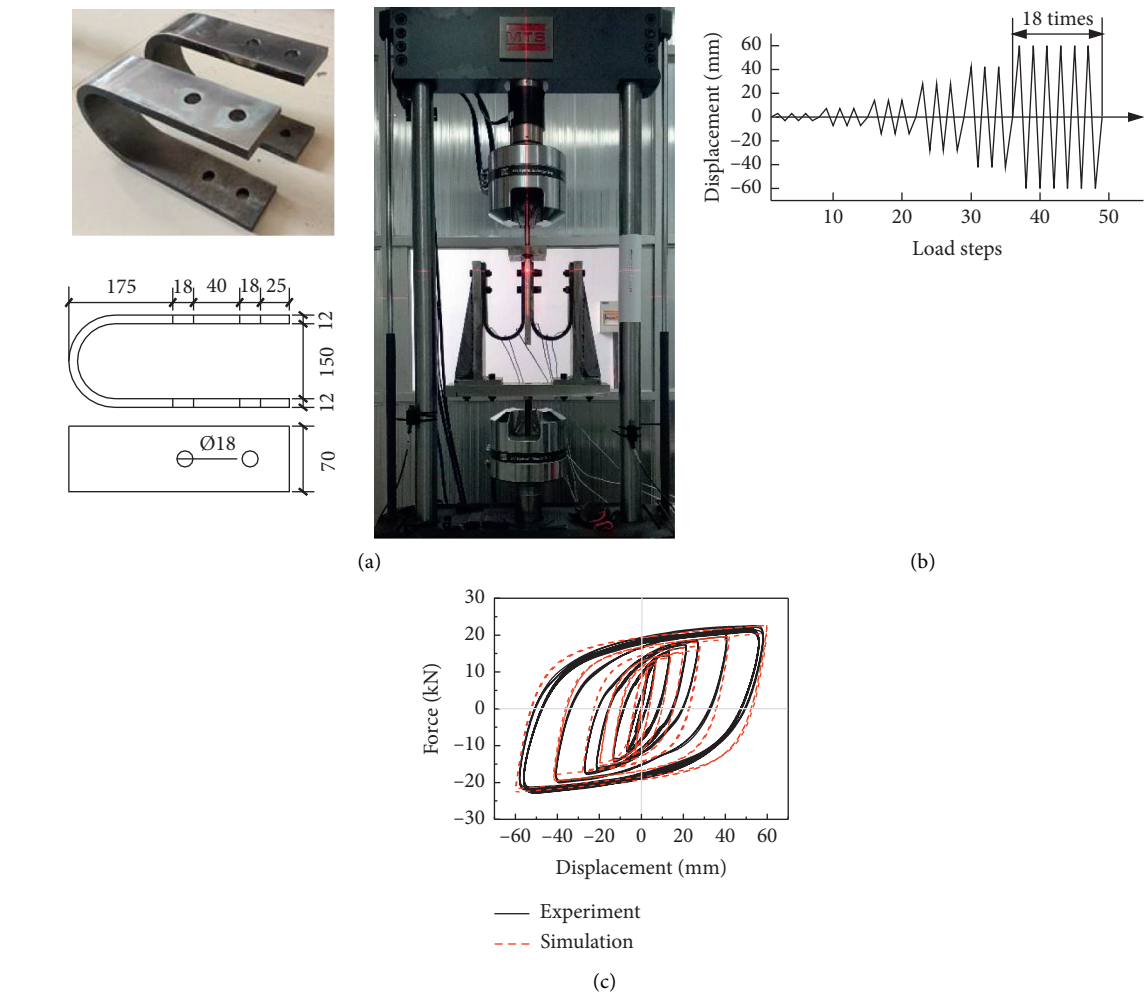

Figure 3: Calibration of the USD finite element model. (a) Loading device and the design of the USD (unit: mm). (b) Loading protocolin the test. (c) Comparison of the simulations and experiments.

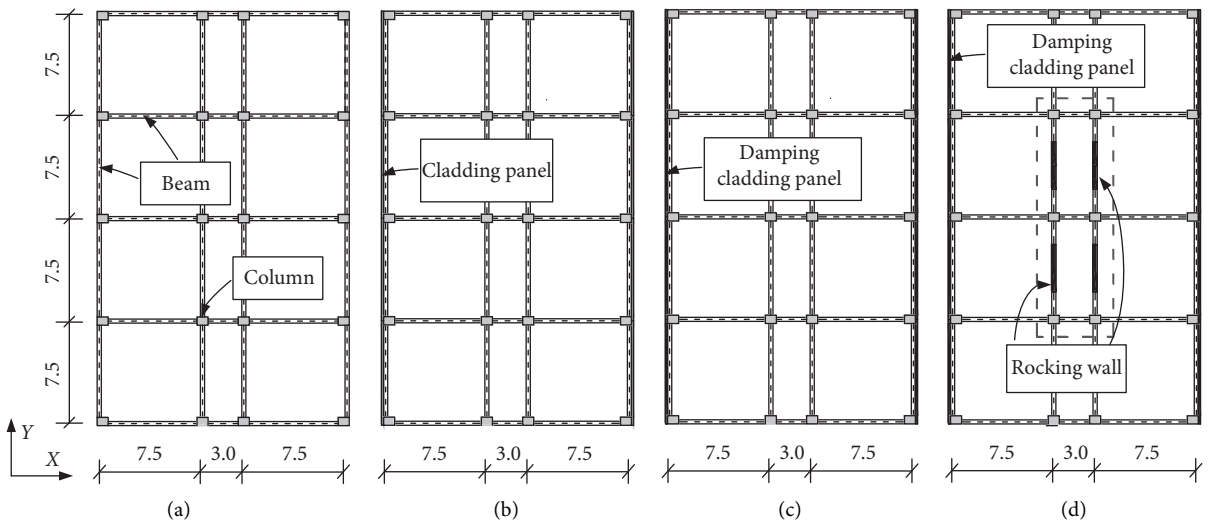

Figure 4: Benchmark model and three kinds of contrast models (unit: m). (a) Benchmark model. (b) PRCFCP. (c) PRCFCP-USD. (d) PRCFCP-USD-RW.

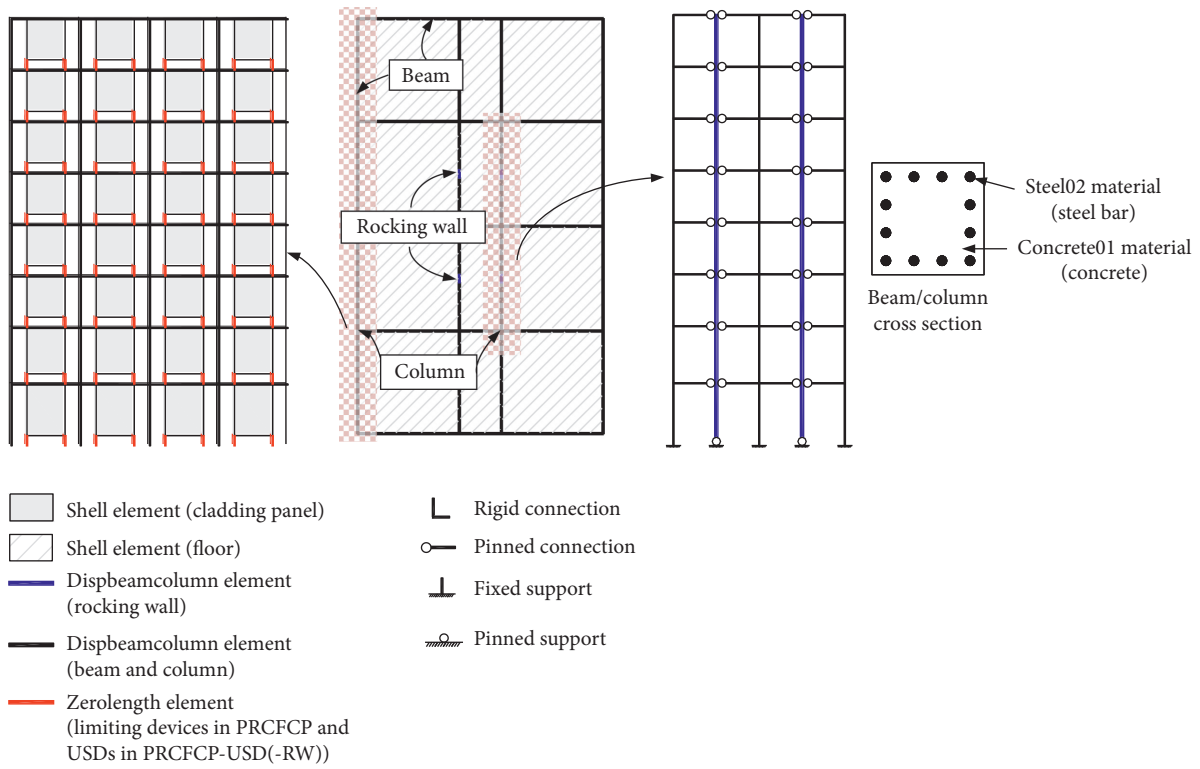

Figure 5: Numerical models used in this paper.

RW use one zero-length element to simulate two USDs; therefore, the stiffness and yield force are twice the one USD shown in Figure 3(c). The initial elastic stiffness in the PRCFCP is deliberately set to infinity for the purpose of simulating the free sliding of the cladding panels. The beam/column and beam/rocking walls joints use rigid connections and pinned connections, respectively.

The model mass is added to each storey node in the form of a concentrated mass. The lateral load is an inverted triangle mode in nonlinear pushover analyses, and the Rayleigh damping with natural damping ratio is 0.05 in the nonlinear dynamic time-history analyses. The seismic lateral loads act on the structural Y direction. All nonlinear analyses consider the P-delta effect of gravity. The fundamental periods (T_1) of the benchmark model and three contrast models are shown in Table 1.

3.4. Ground Motions Selection. The dynamic time-history analyses use 22 ground motions recommended in [26], as reported in Table 2. Figure 6 shows the acceleration response spectra for 22 ground motions-adjusted acceleration peaks to 4 m/s^2 and the acceleration design spectrum corresponding to the major earthquake specified by the Chinese code (GB 50011–2010) [34]. The average and design spectrum accelerations (S_a) are similar. This paper focuses on the average value of the structural responses under 22 ground motions. Since the three contrast models have a large response under the 9th ground motion (GM9), this paper also focuses on the performance differences of the comparison models under the 9th ground motion, and its acceleration time-history curves are shown in Figure 7.

4. Nonlinear Pushover Analyses

Figure 8 shows curves of the base shear force and the roof displacement for the contrast models under inverted triangle lateral load. The curve slope of the PRCFCP-USD is slightly larger than that of the PRCFCP before the structures yield. Therefore, the PRCFCP-USD exhibits a slightly larger lateral stiffness than the PRCFCP, indicating that the addition of the USD can improve the structural stiffness to a certain extent. The lateral load-carrying capacity of the PRCFCP-USD is also slightly larger than that of the PRCFCP, and their base shear forces show a significant downward trend after they reach the peak lateral load-carrying capacity. Figure 8 also shows that the curve slopes of the PRCFCP-USD and PRCFCP-USD-RW structures basically remain consistent before the structures yield, which is mainly because the addition of rocking walls cannot change the lateral stiffness of the structures. Notably, the lateral load-carrying capacity of the PRCFCP-USD-RW is unchanged and is significantly larger than that of the PRCFCP-USD as the loading continues. This result indicates that the lateral load-carrying capacity and ductility of the PRCFCP-USD are enhanced by the participation of the rocking walls.

Figures 9(a)–9(c) show curves of the storey shear force and the storey drift ratio of the frames in the contrast models under the structural pushover. Notably, the interstorey shear force is the sum of the shear forces of all frame columns.

Table 1: Periods of all models (the values in brackets are the modal mass participating ratios).

Models	Reference [31]	Benchmark model	PRCFCP	PRCFCP -USD	PRCFCP -USD-RW
T_1 (s)	1.169	1.118 (0.825)	1.051 (0.840)	0.915 (0.861)	0.910 (0.951)

Table 2: 22 ground motions recommended in [26].

Number	Earthquake	Year	Component	Magnitude (M)	PGA (m/s^2)
1	Friuli, Italy-01	1976	A-TMZ270	6.50	2.93
2	Imperial Val.-06	1979	H-DLT352	6.53	3.44
3	Imperial Val.-06	1979	H-PTS315	6.53	2.00
4	Superst. Hills-02	1987	B-IVW360	6.54	1.82
5	Loma Prieta	1989	G03090	6.93	3.60
6	Loma Prieta	1989	HDA165	6.93	2.07
7	Loma Prieta	1989	HSP000	6.93	3.63
8	Landers	1992	CLW - TR	7.28	3.04
9	Landers	1992	JOS090	7.28	2.78
10	Landers	1992	YER270	7.28	1.65
11	Northridge-01	1994	LOS270	6.69	4.72
12	Northridge-01	1994	ORR090	6.69	5.57
13	Northridge-01	1994	STM090	6.69	7.38
14	Kobe, Japan	1995	KAK090	6.90	3.38
15	Kobe, Japan	1995	SHI000	6.90	2.38
16	Duzce, Turkey	1999	BOL090	7.14	8.06
17	Chichi, Taiwan-05	1999	TCU029-N	7.62	1.97
18	Chichi, Taiwan-05	1999	TCU070-E	7.62	2.50
19	Chichi, Taiwan-05	1999	TCU095-E	7.62	3.35
20	Wenchuan	2008	UA0097	8.00	4.59
21	Wenchuan	2008	UA0103	8.00	2.79
22	Wenchuan	2008	UA0196	8.00	3.23

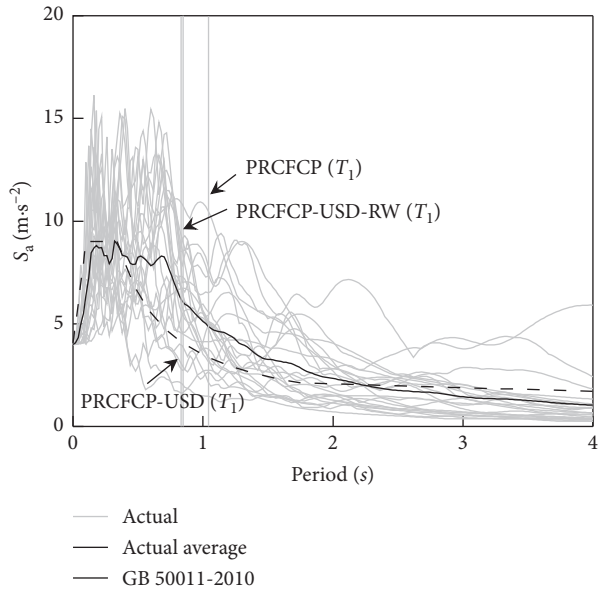

Figure 6: Comparison between the design spectrum and the spectra of actual ground motions.

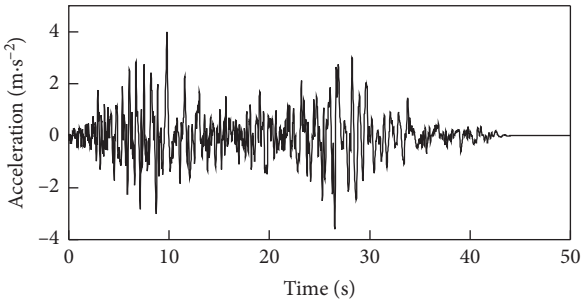

Figure 7: Acceleration time-history curve for GM9.

Figure 9(d) shows curves of interstorey drift ratio when the structures arrived at the peak lateral load-carrying capacity.

A drift concentration factor (DCF) was defined by [35] as (1) for the purpose of evaluating the structural lateral deformation mode and damage concentration degree. The parameter $\theta_{\max}$ is the maximum interstorey drift ratio, u_{roof} is the structural roof displacement, and H is the structural total height. If $DCF = 1$, the structural interstorey drift at each storey is identical. When structures arrive at the peak lateral load-carrying capacity, the DCF values of three contrast models are also listed in Figure 9(d), where DCF_1-DCF_3 represent the DCF values of the PRCFCP, PRCFCP-USD, and PRCFCP-USD-RW, respectively:

$$DCF = \frac{\theta_{\max}}{u_{\text{roof}}/H}. \tag{1}$$

It can be observed in Figures 9(a) and 9(b) that when structures arrive at the peak lateral load-carrying capacity, the interstorey drift ratios of 1F and 2F are higher than those of 3F–8 F in the PRCFCP and PRCFCP-USD, and the interstorey shear forces of 3F–8 F do not reach their interstorey lateral load-carrying capacities,

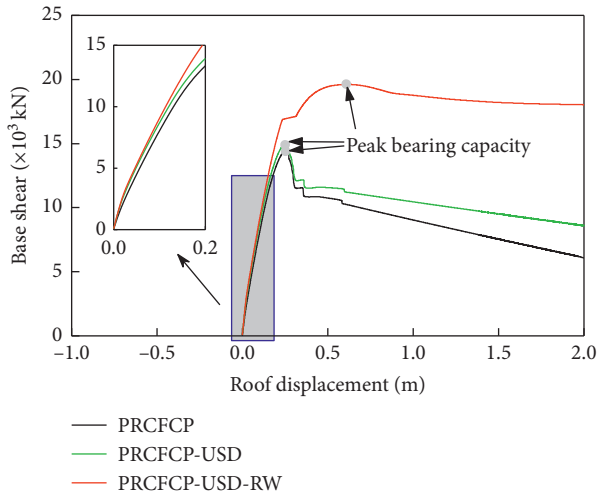

Figure 8: Curves of the base shear force and roof displacement.

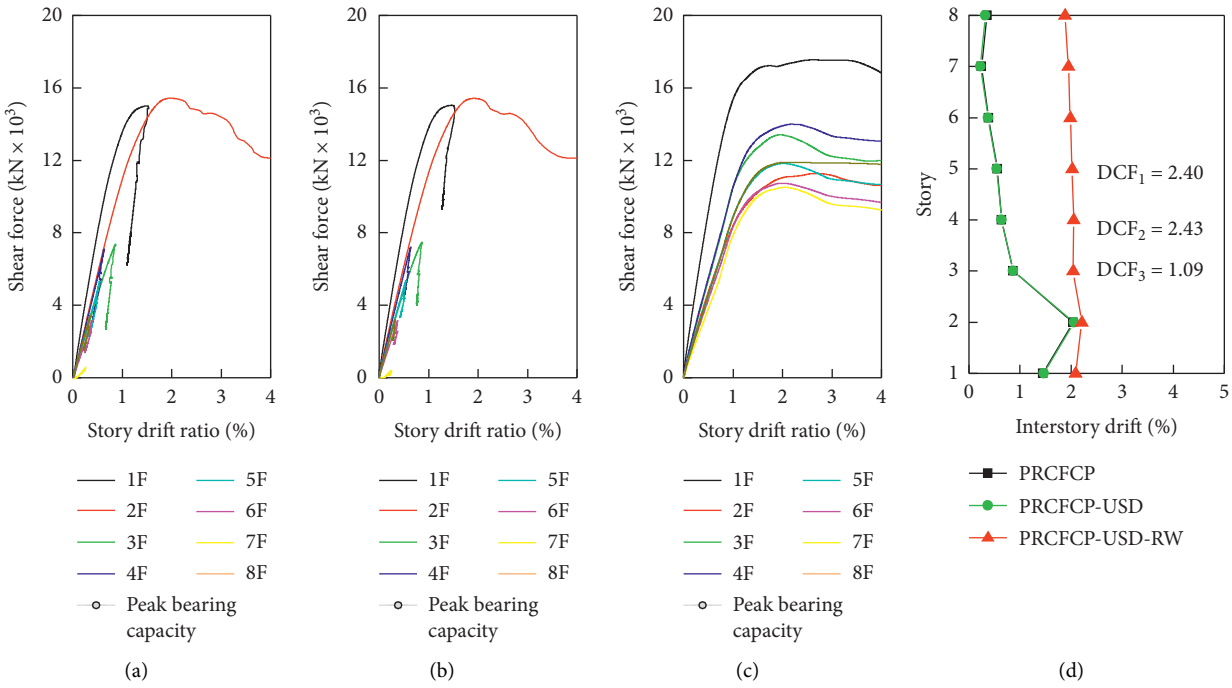

Figure 9: Interstorey shear force and interstorey drift curves of the frame. (a) PRCFCP. (b) PRCFCP -USD. (c) PRCFCP -USD-RW. (d) Inter-storey drift.

implying that these storeys basically maintain the elastic status. The *DCF* values of the PRCFCP and PRCFCP-USD are 2.40 and 2.43, respectively, which means that the damage concentration exists. After the structures arrive at the peak lateral load-carrying capacity, the interstorey drift ratios of 2F in the PRCFCP and PRCFCP-USD are continuously increased as the loading continues; however, the interstorey drift ratios and shear forces of other storeys are slightly and considerably decreased, respectively. These results indicate that the damage of the PRCFCP and PRCFCP-USD is concentrated on the second storey and that the capacities of other storeys cannot be fully used.

Figure 9(c) shows that the interstorey drift ratios at each storey of the PRCFCP-USD-RW are basically the same, and the *DCF* value is only 1.09 when it arrives at the lateral load-carrying capacity. The trends of the interstorey shear force and the drift ratio curves are similar among the different storeys during the whole loading process, and all storeys can enter the plastic phase at the same time. The results indicate that the capacities of all storeys can be fully used due to the addition of rocking walls.

In conclusion, it is difficult to change the structural deformation mode by the use of USDs; however, the addition of rocking wall is an effective way to control the distribution of the interstorey shear force and drift.

5. Nonlinear Dynamic Time-History Analyses

5.1. Peak Interstorey Drift Responses. Figure 10 compares the distributions of the peak interstorey drift ratios for the contrast models under major earthquakes. The peak interstorey drift ratios of the PRCFCP and PRCFCP-USD exhibit an obvious increase at the second storey, indicating that the structures show an interstorey damage concentration. The average interstorey drift ratio of the PRCFCP is close to the allowable limit (2%) [27]. A comparison of Figures 10(a) and 10(b) shows that the peak interstorey drift ratios of the PRCFCP-USD are less than those of the PRCFCP, which illustrates that USDs arranged in the structure can play a role in energy dissipation to reduce the peak interstorey drift response. Figure 10(c) shows that the peak interstorey drift ratios of the PRCFCP-USD-RW are uniformly distributed and do not exhibit obvious increase or reduction, and the average value is far less than 2%. These results indicate that the USDs and rocking walls of the PRCFCP-USD-RW can work together to render peak interstorey drifts small and uniform.

Figure 11 presents the corresponding *DCF* results of the contrast models under major earthquakes. The *DCF* average values for the PRCFCP, PRCFCP-USD, and PRCFCP-USD-RW under various ground motions are 2.53, 2.50, and 1.19, and their standard deviations are 0.89, 0.49, and 0.09, respectively. These results indicate that the rocking walls can control structural deformation and reduce the randomness of the damage concentration. Compared with the PRCFCP, the *DCF* values of the PRCFCP-USD are larger under some ground motions. In other words, the *DCF* value may be increased, and the unevenness of the interstorey drift distribution may be deepened when the USDs are arranged. This conclusion that the USD cannot control the structural deformation mode is consistent with Figures 9 and 10.

5.2. Hysteresis Responses of the USDs. For the PRCFCP-USD and PRCFCP-USD-RW structures, the USDs at the same position of each storey are selected to check the hysteresis response. Figure 12 shows the USDs' hysteretic curves of the PRCFCP-USD and PRCFCP-USD-RW at each storey under the 9th ground motion. As shown in Figure 12(a), the hysteretic curves of the USDs arranged at 1 F and 2 F are full, and the energy dissipations are overused, in which the USDs may reach their energy limit and be destroyed. The USDs at 3 F–6 F cannot fully use the performance, and the USDs arranged at 7 F and 8 F are in the elastic phase and basically do not dissipate any seismic energy. These results indicate that, compared to the PRCFCP-USD-RW, the PRCFCP-USD is prone to the serious damage concentration in that the USDs yield only at less storeys.

As shown in Figure 12(b), the USDs in the PRCFCP-USD-RW show uniform energy dissipation along the structural height. A comparison of Figures 12(a) and 12(b) shows that the energy dissipation of the USDs at 1 F and 2 F in PRCFCP-USD-RW is less than that of PRCFCP-USD, and this situation is reversed at other storeys. In particular, the USDs placed at 7 F and 8 F in PRCFCP-USD-RW are still able to dissipate energy, indicating that the addition of rocking walls can enable all USDs at each storey to enter the energy dissipation stage by coordinating each storey drift to avoid the waste of the USD performance. The distributions of the USDs' displacement responses at each storey observed from Figures 12(a) and 12(b) are consistent with Figures 10(b) and 10(c), respectively, because the deformation of the USDs is mainly determined by the interstorey drift of the frame. Thus, the distribution of the USDs' energy dissipation at each storey is also consistent with the structural interstorey drifts.

5.3. Dispersion Coefficients. A dispersion coefficient α_i is defined herein as (2) for the purpose of evaluating the level of uneven energy dissipation of the USDs at each storey. The parameter μ_i is the ductility coefficient of the USD at the ith storey, and μ_{ave} is the average value of μ_i, which can be calculated using (3). When α_i is closer to 1, the difference in the USDs' energy dissipation at each storey is less:

$$\alpha_i = \mu_i/\mu_{ave} \quad (i = 1 \sim 8), \tag{2}$$

$$\mu_{ave} = (\mu_1 + \mu_2 + \ldots + \mu_8)/8. \tag{3}$$

Figure 13 shows the distribution of α_i for the PRCFCP-USD and PRCFCP-USD-RW under the 22 ground motions. The α_i of the PRCFCP-USD and PRCFCP-USD-RW falls in the range of 0.5–2.5 and 0.8–1.3, respectively. In other words, the difference in the energy dissipation of the USDs at various storeys in the PRCFCP-USD-RW is less than that of the PRCFCP-USD. Therefore, the addition of rocking walls can control the USDs at various storeys to uniformly dissipate the seismic energy.

5.4. Energy Dissipation. Figure 14 shows a comparison of the total energy dissipation for contrast models under each ground motion. Table 3 gives the average energy dissipation of the frame and USDs in three models under 22 ground motions. The total energy dissipation of the PRCFCP-USD and the PRCFCP-USD-RW is similar. From the foregoing analyses, although the dissipated energy of the USDs at 1 F and 2 F in the PRCFCP-USD-RW is less than that of the PRCFCP-USD, the USDs at other storeys of the PRCFCP-USD-RW can fully dissipate the energy, which further causes the total energy dissipation of the USDs in the PRCFCP-USD-RW to be greater than that of the PRCFCP-USD. The seismic energy dissipation by the frame in the PRCFCP is higher than that in the others, which means that the damage to the frame in the PRCFCP is more serious than that in the PRCFCP-USD and PRCFCP-USD-RW. In addition, the seismic energy dissipation by the frame in the PRCFCP-USD-RW is only 63% of that in the PRCFCP-USD. The result indicates that the combination of USDs and rocking walls can effectively reduce the damage to the main structure.

Figure 15 shows the energy dissipation at each storey of the three contrast models under the 9th ground motion. The seismic energy in the PRCFCP and PRCFCP-USD is mainly

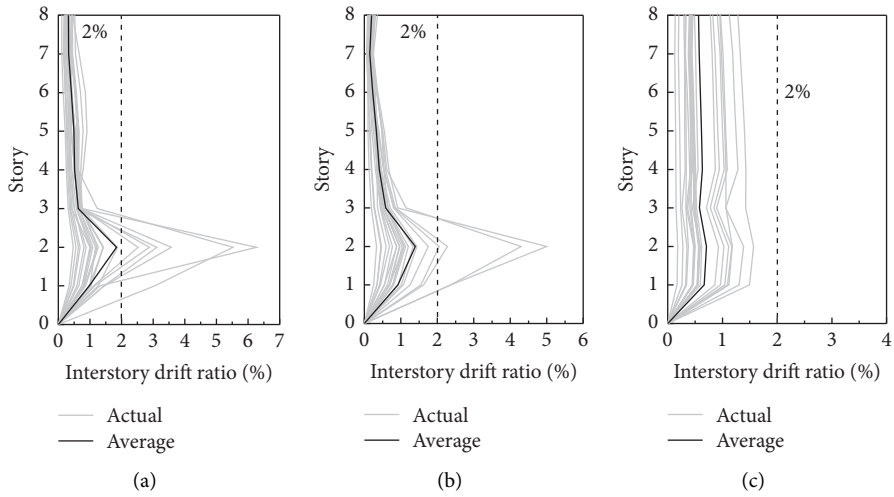

Figure 10: Comparison of the peak interstorey drift distributions under major earthquakes. (a) PRCFCP. (b) PRCFCP -USD. (c) PRCFCP -USD-RW.

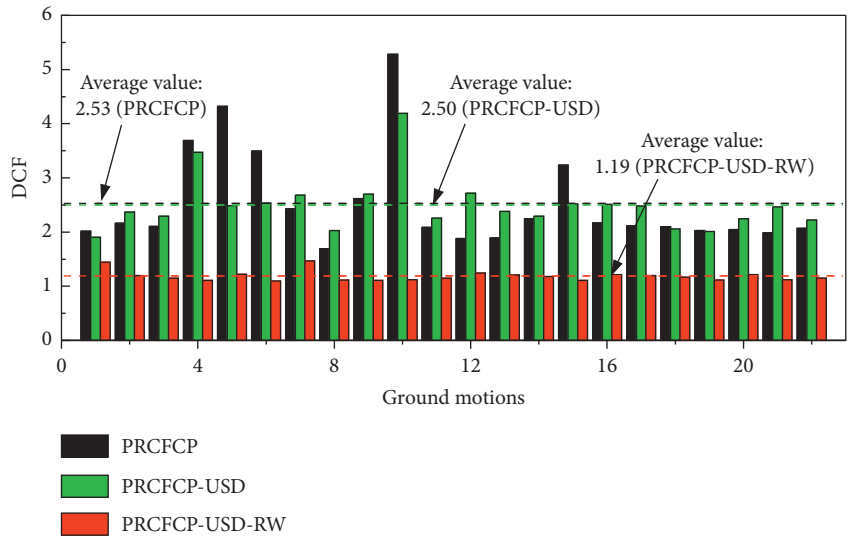

Figure 11: Comparison of the *DCF*s under major earthquakes.

dissipated by the members at the 1–2 storeys, which is a significantly uneven energy dissipation. The frame at storeys 1–2 in the PRCFCP and PRCFCP-USD exhibits severe plastic deformation, while the frame at storeys 6–8 basically maintains flexibility, which means that the PRCFCP-USD exhibits damage concentration. In contrast, the frame and USDs in the PRCFCP-USD-RW roughly consume the same energy at each storey. The damage of the PRCFCP-USD-RW is concentrated in the USDs, and each storey of the frame evenly produces a slight plastic deformation. Compared with the PRCFCP-USD, the PRCFCP-USD-RW exhibits enhanced seismic performance, and the proposed approach of combining the USDs and the rocking walls can protect the main frame to avoid severe destruction and damage concentration.

5.5. Residual Displacement. Figure 16 shows the distributions of the residual interstorey drift ratios of the contrast models under major earthquakes. The largest residual interstorey drift ratio of the PRCFCP occurs at 2F, and the average value is 0.29%, while the values of the PRCFCP-USD and PRCFCP-USD-RW are only 0.075% and 0.031%, respectively. Compared with the PRCFCP, the peak residual interstorey drift ratios of the PRCFCP-USD and PRCFCP-USD-RW are reduced by 74.1% and 89.3%, respectively. These results mean that the residual displacement can be reduced by the participation of USDs, and the rocking walls can enhance the USDs' capacity of reducing the residual displacement. The residual displacement of the PRCFCP-USD-RW is also uniformly distributed at various storeys similar to the peak deformation.

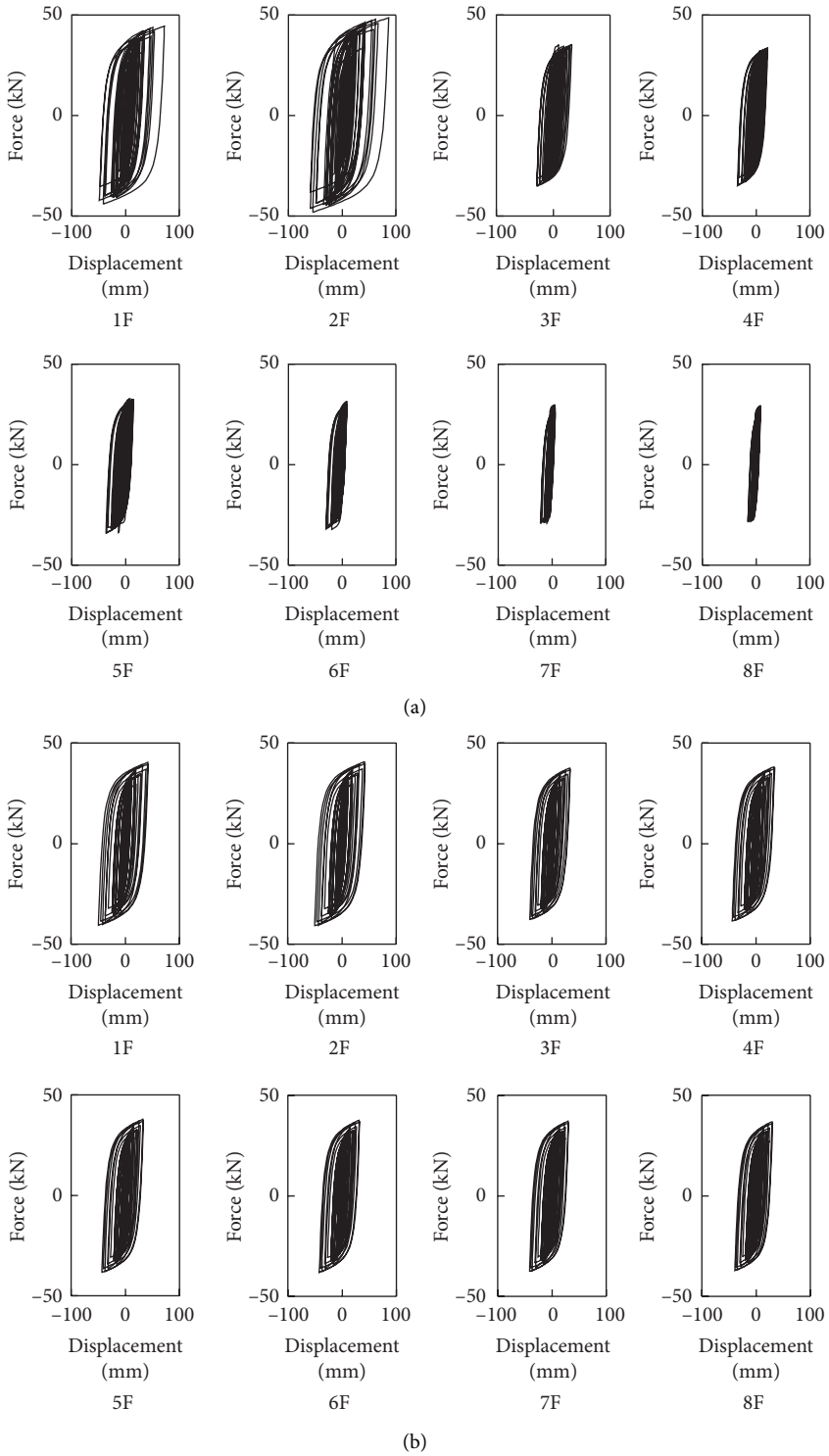

Figure 12: Hysteresis responses of the USDs at different storeys of PRCFCP-USD and PRCFCP-USD-RW under GM9. (a) PRCFCP-USD. (b) PRCFCP-USD-RW.

6. Incremental Dynamic Analyses (IDAs)

6.1. IDA Curves. The seismic collapse capacities of the three contrast models are analysed via the incremental dynamic analysis (IDA) method [36] under the 22 ground motions shown in Section 3.4. The limit interstorey drift ratio of 2.0% specified by ASCE7-10 [37, 38] is used as the sign of the collapse. The approach used to scale the 22 GMs was the hunt&fill algorithm mentioned in [39]. The amplitude modulation and the increment of the step are 0.2 g and 0.05 g, respectively, and the S_a (T_1, 5%) (means the spectral acceleration of the ground motions at the fundamental

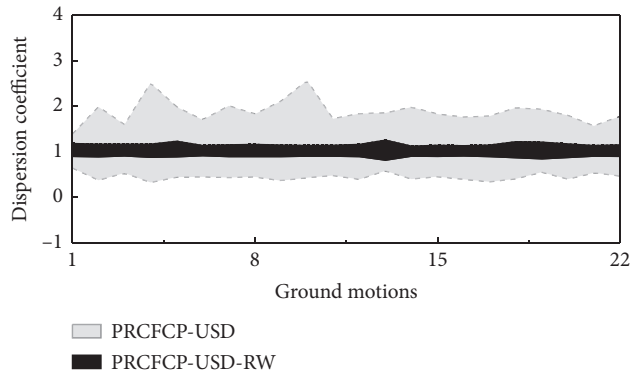

Figure 13: Dispersion coefficients of the USDs energy dissipation under 22 ground motions.

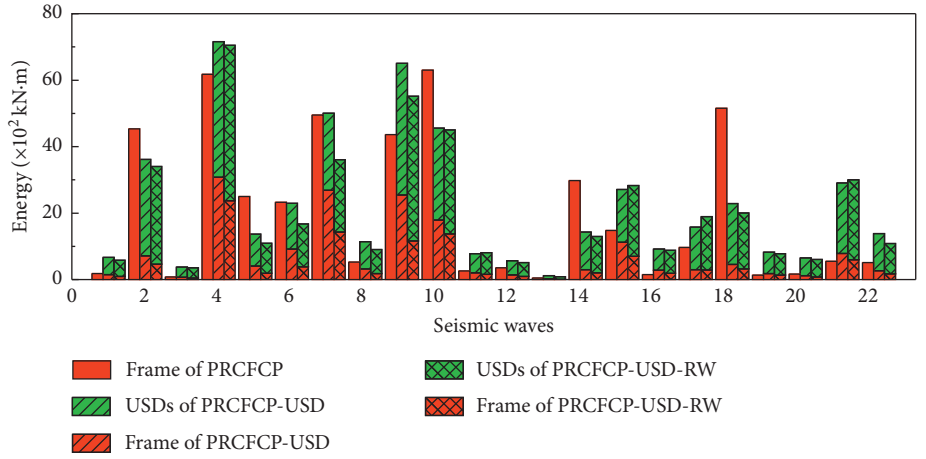

Figure 14: Comparison of the total energy dissipation under 22 ground motions.

Table 3: Average energy dissipation of the frame and USDs under 22 ground motions (unit: kN·m).

	PRCFCP-USD	PRCFCP -USD-RW	PRCFCP -USD-RW/PRCFCP -USD (%)
Frame	766.85	483.92	63
USDs	1454.87	1538.09	106
Total	2221.72	2022.01	91

period of the structure corresponding to 5% damping ratio) of the first analysis step is 0.005 g. The amplitude modulation coefficient (λ_i) and the inputting acceleration of 22 ground motions used in the analyses (S_a') can be calculated using (4) and (5), respectively:

$$\lambda_i = S_a(T1, 5\%)/S_{GT}, \tag{4}$$

$$\mathrm{Sa}' = \lambda_i \cdot \mathrm{S_a}, \tag{5}$$

where S_{GT} is the spectral acceleration for 22 ground motions-adjusted acceleration peaks to 4 m/s^2 corresponding to the major earthquake specified by the Chinese code (GB 50011–2010) and S_a is the actual acceleration of the 22 ground motions (the peak S_a was modulated to 1 m/s^2 in this paper).

Figure 17 shows the IDA curves of the three contrast models corresponding to 16%, 50%, and 84% quantile levels. The IDA curves of the PRCFCP corresponding to three quantile levels are lower than those of the PRCFCP-USD and PRCFCP-USD-RW, indicating that the addition of USDs can improve the seismic collapse capacity. The IDA curve of the PRCFCP-USD-RW is significantly higher than that of the PRCFCP-USD, which reveals that the rocking walls can further improve the structural seismic collapse capacity.

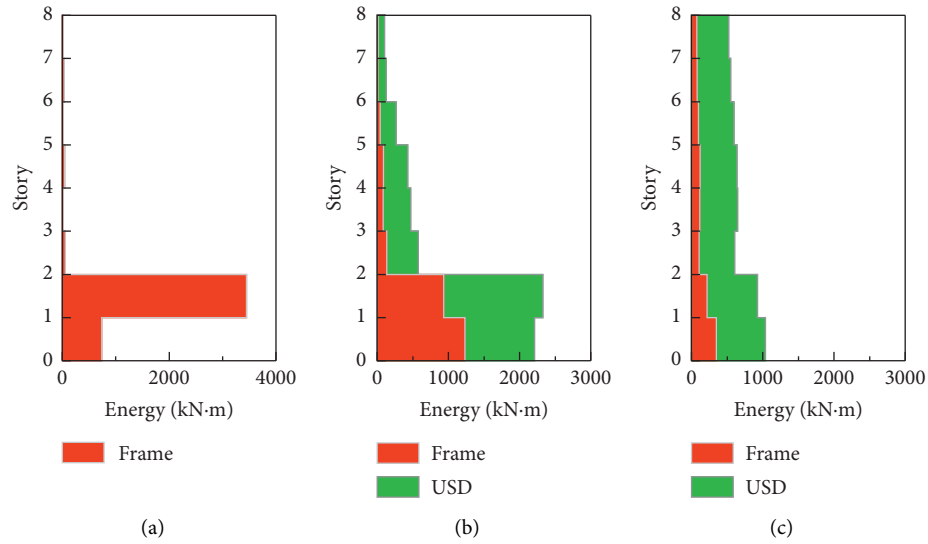

Figure 15: Energy dissipation at different storeys under GM9.

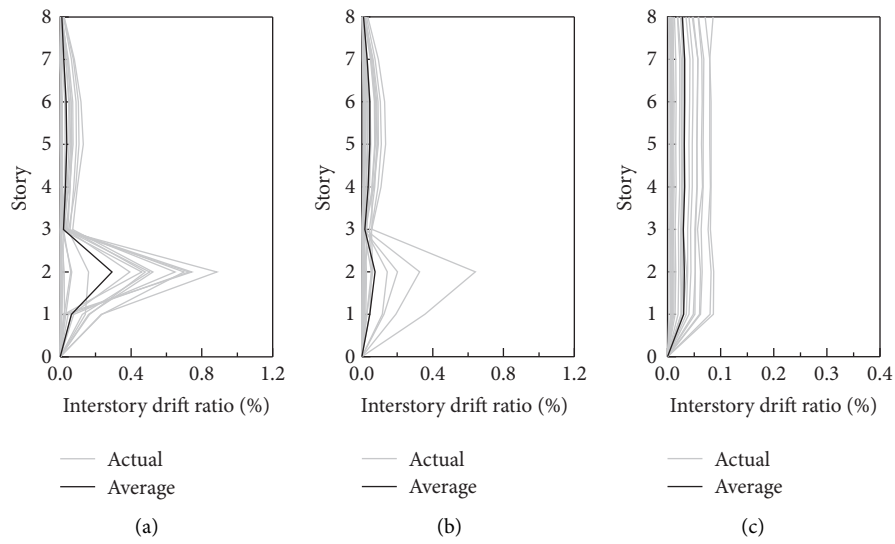

Figure 16: Comparison of the residual interstorey drifts under major earthquakes. (a) PRCFCP. (b) PRCFCP -USD. (c) PRCFCP -USD-RW.

6.2. Evaluation of the Seismic Collapse Capacity. The collapse margin ratio (*CMR*), an important index for measuring the structural seismic collapse capacity [40], can be calculated by (6), where $\widehat{S}_{CT}$ is the spectral acceleration corresponding to the median value of the estimated spectral accelerations at collapse and S_{MT} is the spectral acceleration at the fundamental period of the structure shown in Figure 6:

$$CMR = \widehat{S}_{CT}/SMT. \quad (6)$$

Figure 18 shows the comparison of the collapse probability curves for the contrast models. The collapse probability of the PRCFCP-USD and PRCFCP-USD-RW is significantly smaller than that of the PRCFCP under the same intensity earthquake. Table 4 shows the *CMR* values of the contrast models. The *CMR* value of the PRCFCP-USD is increased by 31.3% compared to the PRCFCP, which means that the seismic collapse capacity can be improved via the addition of USDs. The *CMR* of the PRCFCP-USD-RW is increased by 152.8%, which is approximately five times that of 31.3%, which means that the participation of rocking walls further improves the seismic collapse capacity of the PRCFCP-USD.

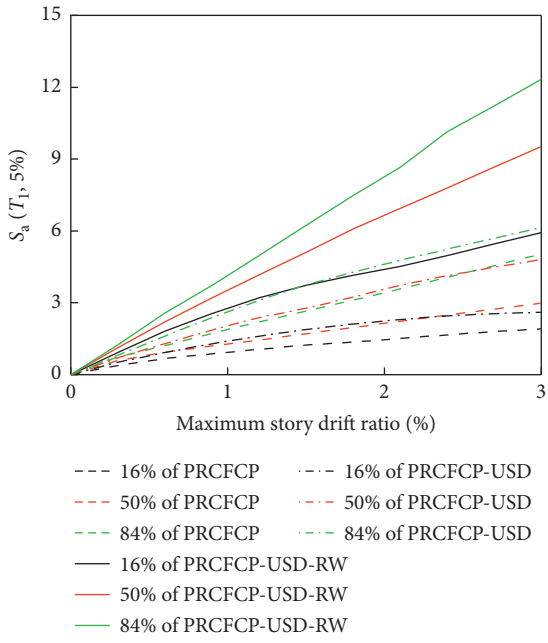

Figure 17: Comparison of the three models' IDA curves.

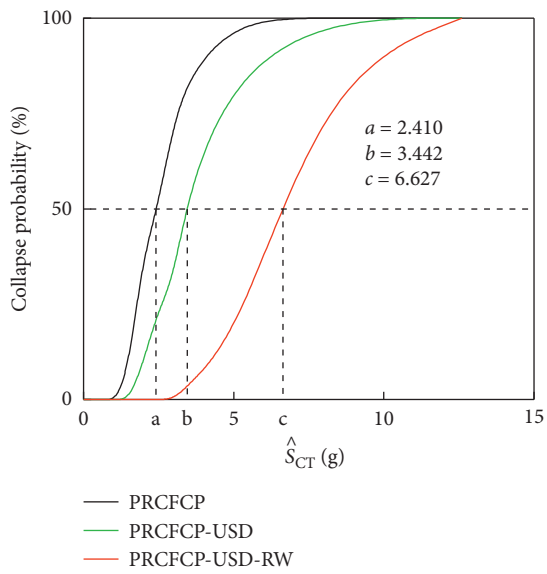

Figure 18: Comparison of the collapse fragility curves among the contrast models.

Table 4: CMR of all models.

Models	$\widehat{S}_{CT}$	S_{MT} (g)	*CMR*	Increase
PRCFCP	2.410 g	0.356	6.77	—
PRCFCP-USD	3.442 g	0.387	8.89	31.3%
PRCFCP-USD-RW	6.627 g	0.387	17.12	152.8%

7. Conclusions

The energy dissipation capacity of the USDs placed between the cladding panels and the main structure and the controlling deformation capacity of rocking walls are combined to improve the seismic performance of the traditional PRCFCP. The following conclusions are obtained through the comparative analyses of the structures with/without the USDs or the rocking walls.

(1) The participation of the USDs can slightly enhance the lateral load-carrying capacity of the structure and slightly reduce the velocity of the carrying reduction after structural yield under a pushover compared with the PRCFCP. However, the combination of rocking walls and USDs can significantly enhance the lateral load-carrying capacity and ductility of the structure.

(2) In PRCFCP-USD, the USDs can dissipate energy and effectively reduce the deformation of the structure under an earthquake, indicating that the cladding panel with USDs can achieve the target of shock absorption.

(3) The USDs at each storey of the PRCFCP-USD exhibit a large difference in energy dissipation. In the position where the interstorey drift is sufficient, the USDs dissipate energy in excess. In places with smaller drifts, the USDs' capacity cannot entirely perform. Rocking walls can compel the USDs at each storey to evenly dissipate energy.

(4) Compared with the PRCFCP, the *DCF* values of the PRCFCP-USD are larger under some ground motions because the USDs at each storey unevenly dissipate energy. In the PRCFCP-USD-RW, the peak interstorey drift and residual displacement are small and uniform, and the *DCF* average value is only 1.19. According to conclusions (2)–(4), the use of USDs can reduce the structural displacement response but not control the structural deformation profile; however, the two design goals can be simultaneously achieved through the combination of rocking walls and USDs.

(5) The seismic collapse capacity of the PRCFCP-USD and PRCFCP-USD-RW is larger than that of the PRCFCP. The *CMR* value of the PRCFCP-USD-RW is approximately five times that of the PRCFCP-USD, showing that the seismic collapse capacity can be improved by the proposed cladding panels with USDs and that the combination of rocking walls and USDs further improves the seismic collapse capacity.

Data Availability

The authors declare that all data supporting the findings of this study are available within the article.

Conflicts of Interest

The authors declare no conflicts of interest.

Acknowledgments

This research was financially supported by the National Natural Science Foundation of China (nos. 51708166,

51778201, and 51878233), the Fundamental Research Funds for Central Universities of China (no. JZ2019HGTB0086), and the China Postdoctoral Science Foundation (no. 2018M630706). Their support is gratefully acknowledged.

References

[1] H. Maneetes, "Development of a seismic dissipating mechanism for precast concrete cladding panels," Ph.D. Dissertation, Pennsylvania State, University, State College, PA, USA, 2007.

[2] E. D. Losch, P. W. Hynes, R. Andrews Jr. et al., "State of the art of precast/prestressed concrete sandwich wall panels," *PCI Journal*, vol. 56, no. 2, pp. 131–176, 2011.

[3] Precast/Prestressed Concrete Institute, *PCI Design Handbook*, Precast/Prestressed Concrete Institute, Chicago, IL 60606, USA, 7th edition, 2010.

[4] JGJ/T458-2018, *Technical standard for application of precast concrete facade panel*, China Building Industry Press, Beijing, USA, 2018, in Chinese.

[5] A. Belleri, E. Brunesi, R. Nascimbene et al., "Seismic performance of precast industrial facilities following major earthquakes in the Italian territory," *Journal of Performance of Constructed Facilities*, vol. 29, no. 5, Article ID 04014135, 2014.

[6] G. Toniolo and A. Colombo, "Precast concrete structures: the lessons learned from the L'Aquila earthquake," *Structural Concrete*, vol. 13, no. 2, pp. 73–83, 2012.

[7] D. A. Bournas, P. Negro, and F. F. Taucer, "Performance of industrial buildings during the Emilia earthquakes in Northern Italy and recommendations for their strengthening," *Bulletin of Earthquake Engineering*, vol. 12, no. 5, pp. 2383–2404, 2014.

[8] GCR Nist 96-681, *Literature Review on Seismic Performance of Building Cladding Systems*, National Institute of Standards and Technology, United States Department of Commerce, Gaithersburg, MD, USA, 1995.

[9] R. Tyler, "Damping in building structures by means of PTFE sliding joints," *Bulletin of New Zealand National Society for Earthquake Engineering*, vol. 10, no. 3, pp. 139–142, 1977.

[10] J. M. Cohen and G. H. Powell, "A design study of an energy-dissipating cladding system," *Earthquake Engineering & Structural Dynamics*, vol. 22, no. 7, pp. 617–632, 1993.

[11] J.-P. Pinelli, C. Moor, J. I. Craig, and B. J. Goodno, "Testing of energy dissipating cladding connections," *Earthquake Engineering & Structural Dynamics*, vol. 25, no. 2, pp. 129–147, 1996.

[12] L. Ferrara, R. Felicetti, G. Toniolo, and C. Zenti, "Friction dissipative devices for cladding panels in precast buildings," *European Journal of Environmental and Civil Engineering*, vol. 15, no. 9, pp. 1319–1338, 2011.

[13] A. Baird, A. Palermo, and S. Pampanin, "Controlling seismic response using passive energy dissipating cladding connections," in *Proceedings of the New Zealand Society for Earthquake Engineering Conference*, Wellington, New Zealand, April 2013.

[14] P. Negro and M. Lamperti Tornaghi, "Seismic response of precast structures with vertical cladding panels: the safe-cladding experimental campaign," *Engineering Structures*, vol. 132, pp. 205–228, 2017.

[15] B. Dal Lago, F. Biondini, and G. Toniolo, "Experimental investigation on steel W-shaped folded plate dissipative connectors for horizontal precast concrete cladding panels," *Journal of Earthquake Engineering*, vol. 22, no. 5, pp. 778–800, 2018.

[16] B. Dal Lago, F. Biondini, and G. Toniolo, "Experimental tests on multiple-slit devices for precast concrete panels," *Engineering Structures*, vol. 167, pp. 420–430, 2018.

[17] F. Karadoğan, E. Yüksel, A. Khajehdehi et al., "Cyclic behavior of reinforced concrete cladding panels connected with energy dissipative steel cushions," *Engineering Structures*, vol. 189, pp. 423–439, 2019.

[18] B. Alavi and H. Krawinkler, "Strengthening of moment-resisting frame structures against near-fault ground motion effects," *Earthquake Engineering & Structural Dynamics*, vol. 33, no. 6, pp. 707–722, 2004.

[19] Z. Qu, A. Wada, S. Motoyui, H. Sakata, and S. Kishiki, "Pin-supported walls for enhancing the seismic performance of building structures," *Earthquake Engineering & Structural Dynamics*, vol. 41, no. 14, pp. 2075–2091, 2012.

[20] G. Deierlein, H. Krawinkler, X. Ma et al., "Earthquake resilient steel braced frames with controlled rocking and energy dissipating fuses," *Steel Construction*, vol. 4, no. 3, pp. 171–175, 2011.

[21] A. Wada, Z. Qu, S. Motoyui, and H. Sakata, "Seismic retrofit of existing SRC frames using rocking walls and steel dampers," *Frontiers of Architecture and Civil Engineering in China*, vol. 5, no. 3, pp. 259–266, 2011.

[22] K. M. Twigden and R. S. Henry, "Experimental response and design of O-connectors for rocking wall systems," *Structures*, vol. 3, pp. 261–271, 2015.

[23] Z. Zhang, R. B. Fleischman, J. I. Restrepo et al., "Shake-table test performance of an inertial force-limiting floor anchorage system," *Earthquake Engineering & Structural Dynamics*, vol. 47, no. 10, pp. 1987–2011, 2018.

[24] Y. Feng, Z. Zhang, X. Chong, J. Wu, and S. Meng, "Elastic displacement spectrum-based design of damage-controlling BRBFs with rocking walls," *Journal of Constructional Steel Research*, vol. 148, pp. 691–706, 2018.

[25] N. Rahgozar, N. Rahgozar, and A. S. Moghadam, "Controlled-rocking braced frame bearing on a shallow foundation," *Structures*, vol. 16, pp. 63–72, 2018.

[26] J. M. Kelly, R. I. Skinner, and A. J. Heine, "Mechanisms of energy absorption in special devices for use in earthquake resistant structures," *Bulletin of NZ Society for Earthquake Engineering*, vol. 5, no. 3, pp. 63–88, 1972.

[27] S. Bagheri, M. Barghian, F. Saieri, and A. Farzinfar, "U-shaped metallic-yielding damper in building structures: seismic behavior and comparison with a friction damper," *Structures*, vol. 3, pp. 163–171, 2015.

[28] S. Mazzoni, F. McKenna et al., *OpenSees Command Language Manual*, PEER, University of California, Berkeley, CA, USA, 2006.

[29] GB 50017-2003, *Code for Design of Steel Structures*, China Planning Press, Beijing, China, 2003, in Chinese.

[30] A. I. Dimopoulos, T. L. Karavasilis, G. Vasdravellis, and B. Uy, "Seismic design, modelling and assessment of self-centering steel frames using post-tensioned connections with web hourglass shape pins," *Bulletin of Earthquake Engineering*, vol. 11, no. 5, pp. 1797–1816, 2013.

[31] Z. Qu, *Study on Seismic Damage Mechanism Control and Design of Rocking Wall-Frame structures*, Tsinghua University, Beijing, China, Ph.D. Dissertation in Chinese, 2010.

[32] M. Palermo and T. Trombetti, "Experimentally-validated modelling of thin RC sandwich walls subjected to seismic loads," *Engineering Structures*, vol. 119, pp. 95–109, 2016.

[33] E. Brunesi, R. Nascimbene, and A. Pavese, "Mechanical model for seismic response assessment of lightly reinforced concrete walls," *Earthquakes and Structures*, vol. 11, no. 3, pp. 461–481, 2016.

[34] GB 50011-2010, *Code for Seismic Design of Buildings*, China Architecture & Building Press, Beijing, China, 2010, in Chinese.

[35] G. A. MacRae, Y. Kimura, and C. Roeder, "Effect of column stiffness on braced frame seismic behavior," *Journal of Structural Engineering*, vol. 130, no. 3, pp. 381–391, 2004.

[36] D. Vamvatsikos and C. A. Cornell, "Incremental dynamic analysis," *Earthquake Engineering & Structural Dynamics*, vol. 31, no. 3, pp. 491–514, 2002.

[37] ASCE, *Minimum Design Loads for Buildings and Other Structures (ASCE/SEI 7-10)*, American Society of Civil Engineers, Reston, VA, USA, 2010.

[38] S. Zaruma and L. A. Fahnestock, "Assessment of design parameters influencing seismic collapse performance of buckling-restrained braced frames," *Soil Dynamics and Earthquake Engineering*, vol. 113, pp. 35–46, 2018.

[39] D. Vamvatsikos and C. A. Cornell, "Tracing and post-processing of IDA curves: theory and software implementation," p.44, Report No. RMS, Stanford University and Stanford, USA, 2001.

[40] Federal Emergency Management Agency (FEMA), *Quantification of building seismic performance factors*, FEMA, Washington, D.C., USA, 2009.